Journal of Catalysis 388 (2020) 30–37

Contents lists available at ScienceDirect

Journal of Catalysis

journal homepage: www.elsevier.com/locate/jcat

Particle size effects in copper-catalyzed hydrogenation of ethyl acetate

Rolf Beerthuis [a], Jan Willem de Rijk [a], Jon M.S. Deeley [b], Glenn J. Sunley [b], Krijn P. de Jong [a], Petra E. de Jongh [a,*]

[a] Inorganic Chemistry and Catalysis, Debye Institute for Nanomaterials Science, Utrecht University, Universiteitsweg 99, 3584 CG Utrecht, Netherlands
[b] Applied Chemistry and Physics Centre of Expertise, BP Group Research, Hull Research and Technology Centre, c/o BP Chemicals, Saltend, Hull, United Kingdom

ARTICLE INFO

Article history:
Received 25 October 2019
Revised 4 May 2020
Accepted 5 May 2020
Available online 19 May 2020

Keywords:
Particle size effects
Copper
Heterogeneous catalysis
Hydrogenation
Carbon

ABSTRACT

Supported Cu catalysts are widely used in the chemical industry. Here, we discuss the role of the Cu particle size in the hydrogenation of ethyl acetate, as a model reaction for Cu-based hydrogenation catalysis and a crucial step to produce ethanol *via* synthesis gas. A series of carbon-supported Cu catalysts was prepared with Cu particle sizes tuned between 3 and 14 nm. At temperatures of 180–210 °C and a pressure of 30 bar, the surface-normalized activity increased around 4-fold when increasing the Cu particle size from 3 to 10 nm, while it became constant for Cu particles above 10 nm, hence showing that the Cu-catalyzed hydrogenation reaction is weakly sensitive to the Cu surface structure. The apparent activation energy for the reaction was around 94 kJ mol^{-1} for all Cu particle sizes, suggesting a size-independent nature of the active sites, whereas the abundance of the active sites increased with increasing Cu particle size below 10 nm. A maximal copper-normalized activity was achieved with Cu particles of around 6 nm, providing an optimal balance between intrinsic activity and available surface area. These findings may guide optimization strategies for reactions where hydrogenation of relatively stable intermediates is the rate-limiting step.

1. Introduction

The catalytic performance for a range of important industrial processes strongly depends on the metal particle size, such as for Co and Fe catalysts in Fischer-Tropsch synthesis [1–3], Pd and Pt for various hydrogenation and oxidation reactions [4,5], and Ag for ethylene epoxidation [6]. Supported Cu catalysts are widely used in industry for methanol synthesis, methane steam reforming, the water-gas shift reaction and numerous oxidation reactions [7]. In the methanol synthesis reaction, a weak but significant particle size effect has been reported [8]. However, the role of the Cu particle size is still not fully understood. This partly originates from the difficulty to control the Cu particle sizes below 10 nm. Additionally, the complexity of many reactions may hamper studies on the correlation between catalyst structure and performance. For example, the methanol synthesis reaction proceeds *via* a combination of concurrent CO hydrogenation, CO_2 hydrogenation and (reverse) water gas shift reactions. To rationally design optimization strategies for Cu-based catalysts in general, it is crucial to understand how the activity, selectivity and stability are affected by varying Cu particle sizes.

The hydrogenation of short chain alkyl esters is a promising model reaction for catalyst studies, since the mechanism is relatively simple and well understood [9–11]. The industrial hydrogenation of esters is commonly performed using Cu-based catalysts. Cu provides distinct advantages over other active hydrogenation metals, *e.g.* Pd, Pt, Ru, Rh and Ni, in the fact that Cu is less expensive, abundantly available and exhibits superior selectivity towards unsaturated C—O ester bonds, leaving C=C bonds intact [12]. Moreover, various alkyl acetates can be efficiently produced *via* synthesis gas. Considering that synthesis gas can be produced from natural gas, coal or renewable biomass and solid municipal waste stream, the conversion of alkyl acetates presents a potential key step to develop more renewable routes towards essential alcohols [13–16]. The hydrogenation of ethyl acetate (EtOAc) is a particularly promising model reaction to investigate the Cu particle size effects, due to the characteristic high selectivity towards ethanol (~95%) [10,14,17,18].

The establishment of structure-performance relationships is facilitated by using well-defined model catalysts, using moderate metal loadings (<20 wt%) and relatively inert support materials [19,20]. To effectively use the metal atoms, a nanometer-sized metal phase is typically desired for catalysis. Interestingly, the catalyst activity is often influenced by the size and structure of metal particles below ~20 nm [21]. In the crucial size regime between 2

* Corresponding author.
E-mail address: P.E.deJongh@uu.nl (P.E. de Jongh).

https://doi.org/10.1016/j.jcat.2020.05.006
0021-9517/

and 10 nm, the various surface facets exhibit a steeply changing fraction of different adsorption sites, such as edges, corners, steps and kinks, with lower metal-metal coordination saturation than terrace sites at flat surfaces [1,22]. Studies on particle size effects for other hydrogenation metals, such as Fe and Co in Fischer Tropsch synthesis [2,3], Ni and Co in CO to methane hydrogenation [21,23], Pd, Pt, Au and Ag for various hydrogenation and oxidation reactions [24–26], demonstrated that the intrinsic activity per surface site was correlated to the size-dependent surface structure of the specific metal nanoparticles [1,8,21,24].

As mentioned above, the Cu-based activity in methanol synthesis from CO and CO_2 depends on the Cu particle size below 10 nm [8]. However, the chemical reactivity does not only depend on the metal size, but also on the chemical nature of the reactant [21,27,28]. An ester bond consists of σ C—O and π C═O bonds, and is different from the π bonds in CO or CO_2. Interestingly, the hydrogenation of the acyl reaction intermediates was reported as the rate-determining step in alkyl ester hydrogenation [10,14,29], which resembles formate hydrogenation as the rate-determining step in the methanol synthesis reaction [30,31]. Unraveling the origin of the Cu particle size effects in the hydrogenation of EtOAc may hence be relevant for a range of Cu-catalyzed reactions.

In addition, there is a debate on the role of the Cu oxidation state. The presence of Cu^+ species was reported to enhance the catalytic activity in the hydrogenation of alkyl acetate [14,18,32], and di-esters [33,34]. It was hypothesized that a combination of dissociative H_2 adsorption on Cu^0 sites and polarization of the C═O ester bond on Cu^+ sites enhanced the catalytic activity [14,18,32,35]. Alternatively, the catalytic activity was reported to scale proportionally with the metallic Cu surface area, in the hydrogenation of dimethyl maleate [36] and dimethyl oxalate [35]. The effects of oxidation state for Cu-based catalysts, and how these scale with Cu particle size, are hence still unclear, and will be taken into account in this study.

We prepared a series of supported Cu catalysts with Cu particle sizes tuned between 3 and 14 nm, and studied whether the hydrogenation of EtOAc was sensitive to the Cu particle size. Additionally, the influence of the initial Cu particle size, poly-dispersity and interparticle distance on the particle growth was evaluated. High surface area graphite was used as the catalyst support, to minimize the metal–support interaction and reveal the intrinsic Cu particle size effects [37].

2. Experimental methods

2.1. Cu/C catalyst preparation

A series of carbon-supported Cu (Cu/C) catalysts was prepared by incipient wetness impregnation using 2.0–3.3 M aqueous Cu $(NO_3)_2$ solutions, followed by drying and thermal treatment to decompose the Cu precursor. The Cu particle size was controlled by a combination of synthesis approaches, including variation of the Cu loading (6–16 wt%) and final heat treatment temperature (250–400 °C), as well as functionalization of the carbon support (liquid phase surface-oxidation using concentrated HNO_3 oxidation for 110 min at 80 °C). High surface area graphite was used as the carbon support (HSAG–500, kindly provided by Timcal Ltd.). The BET specific surface area was approximately 500 m^2 g^{-1}, with a total pore volume of 0.7 mL g^{-1} and a density of acidic surface groups of 0.16 nm^{-2}. The oxidized graphite support had a surface area of approximately 440 m^2 g^{-1}, a total pore volume of 0.62 mL g^{-1} and a density of acidic surface groups of 0.64 nm^{-2}. Further details about the synthesis procedures are described in Section S1 of the Supporting Information.

As an example of a typical synthesis procedure, a Cu/C catalyst containing 16.4 wt% Cu was prepared by impregnating ~2 g of a powdered carbon support to incipient wetness, in a three-necked round-bottom flask. An aqueous solution of 5.0 M $Cu(NO_3)_2$ in 0.1 M HNO_3 (pH ~1) was added drop-wise *via* a syringe through a septum, while stirring under vacuum. The impregnate was stirred for 24 h to advance the uniform distribution of the metal precursor throughout the support. Subsequently, the sample was dried overnight at room temperature, while stirring under dynamic vacuum. The dried sample was transferred to an Ar-filled glovebox and loaded into a tubular flow reactor. Next, the sample was heated with 0.5 °C min^{-1} to 230 °C with 1 h hold with 230 °C under a flow of 5 vol% H_2/N_2 flow (~100 mL min^{-1} g^{-1}; GSHV ~4000 h^{-1}), resulting in decomposition of the nitrate precursor and formation of Cu nanoparticles. Finally, the catalyst was passivated by exposing it overnight to air at room temperature. The final Cu weight loading was calculated as Cu $wt\% = \left(\frac{\text{mass Cu}}{\text{mass CuO+mass support}}\right) * 100\%$. The Cu/C catalysts in this study were denoted as *X*_Cu/Y, in which *X* represents the surface-averaged Cu particle size in nm, as determined by TEM, and *Y* indicates the type of carbon support material.

2.2. Catalyst characterization

TEM and XRD were used as characterization techniques to determine the Cu particle and crystallite sizes and estimate the geometric Cu surface area. Herein, the particles were assumed to be spherical and fully accessible.

Transmission electron microscopy (TEM) was performed on an FEI Tecnai 20 microscope, operated at 200 kV. Samples were prepared by dispersing the dry catalyst powder onto a Ni sample grid, coated with holey carbon (Agar 300 mesh Ni). The Cu particle size was measured for at least 200 individual particles. The number-averaged Cu particle size (d_n, also referred to as d [1,0]) and surface-averaged Cu particle size (d_s, also referred to as d [3,2]), including the standard deviation in the particle size distribution (σ), were calculated using the formulas $d_n \pm \sigma_{dn} = \frac{1}{N}\sum_{i=1}^{N} d_i \pm \sqrt{\frac{1}{N}\sum_{i=1}^{N}(d_n - d_i)^2}$ and $d_s \pm \sigma_{ds} = \frac{\sum_{i=1}^{N} d_i^3}{\sum_{i=1}^{N} d_i^2} \pm \sqrt{\frac{1}{N}\sum_{i=1}^{N}(d_s - d_i)^2}$, in which d_i indicates the diameter of the i^{th} particle and N stands for the total number of measured particles. Methods for calculating the interparticle distance are discussed in Section S1.

X-ray diffractometry was performed on a Bruker D8 powder X-ray diffractometer equipped with a Co-$K_{\alpha 1,2}$ radiation source (λ = 1.79026 Å) and a Lynxeye detector. Diffractograms were taken directly after the final step in the synthesis under reductive atmosphere, or after an additional reduction treatment (1 h at 250 °C in 20 vol% H_2/N_2, ~100 mL min^{-1} g^{-1}), without exposure to air. The reduced catalyst was loaded into an airtight XRD specimen holder (A100B33, Bruker AXS) inside an Ar-filled glovebox (Mbraun LABmaster, <0.1 ppm H_2O, <0.1 ppm O_2). Diffractograms were continuously acquired with 0.1 °2θ increment between 5 and 95 °2θ, in approximately 2–3 h. The diffractograms were normalized to the peak intensity of the graphitic (0 0 2) diffraction peak at 30.9 °2θ and carbon baseline subtracted. The Cu^0 crystallite size was determined by applying the Scherrer equation to the main Cu^0 (2 0 0) diffraction peak at (59.3 °2θ), with a shape factor k of 0.1 [38].

Temperature-programmed reduction (TPR) profiles were measured on a Micromeritics Autochem II ASAP 2920 apparatus, with H_2 consumption detected by a thermal conductivity detector. Prior to the measurement, the passivated catalysts were dried at 120 °C for 30 min under Ar flow (~1 mL min^{-1} mg_{cat}^{-1}) and left to cool down to 50 °C. Next, the reduction profiles were determined by heating the catalyst with 2 °C min^{-1} to 400 °C, in a flow of 5 vol% H_2/Ar (~1 mL min^{-1} mg_{cat}^{-1}). The reduction profiles were base-line

corrected and normalized to the amount of Cu. The onset temperature was estimated from the intercept of the slope at the first inflection point of the peak with the baseline.

2.3. Catalytic performance

Catalytic experiments were performed on a high-throughput fixed-bed reactor system, equipped with 16 parallel channels (Flowrence®, Avantium N. V.). The catalysts were pelletized (2 cm diameter) using a hydraulic press at 1.5 ton weight, equivalent to 460 bar pressure, ground and sieved to obtain a granulate size of 75–150 μm. All experiments were done using ~6.0 mg of Cu mass per reactor. The required amount of catalyst (30–100 mg) was calculated from the Cu weight loading. The Cu/C catalysts were physically diluted with SiC granulates (212–425 μm). The SiC diluent was pre-treated by washing with HNO_3(aq) (68%; 10 mL g_{SiC}^{-1}) and calcining at 800 °C, to remove any metal or organic contaminants. The volume of the diluted catalyst bed was kept constant at 0.3 mL. The catalyst was loaded into a stainless-steel reactor tube (2.6 mm inner diameter) on top of SiC granules (0.5 mL), which were pre-loaded onto a stainless-steel frit. A hollow glass wool fibre was placed on top of the catalyst bed, up to the entrance of the reactor, to ensure constant vaporization of the liquid reactant.

The Cu/C catalysts were re-reduced *in situ* by heating to 200 °C (2 °C min^{-1}) with 2 h hold at 200 °C, under a flow of 20% H_2/Ar (2 mL min^{-1} per reactor). Subsequently, the temperature was lowered to 140 °C and the reactor was purged for 2 h using a mixture of H_2:He in a 10:1 M ratio (6.2 mL min^{-1} per reactor). Next, the EtOAc feed was introduced in the gas phase (0.6 mL min^{-1} per reactor). The reaction mixture consisted of H_2:He:EtOAc in a 10:1:1 M ratio (6.8 mL min^{-1} total flow per reactor). The GHSV based on the packing density of the diluted catalyst and the total gas flow per reactor was approximately 1350 h^{-1}, and the WHSV was around 325 g_{EtOAc} $g_{Cu}^{-1}h^{-1}$. Next, the pressure was gradually increased during 75 min to 30 bar(g). Finally, the temperature was increased to 180 °C with 2 °C min^{-1} to start the catalytic experiment. Between isothermal stages, the temperature was increased with 1 °C min^{-1}. After the reaction, the catalysts were left to cool down to 90 °C and passivated by exposure to air at this temperature.

The Cu-normalized time yield (CTY, mol_{EtOAc} $g_{Cu}^{-1}h^{-1}$) was used to calculate the turn-over frequency (TOF, mol_{EtOAc} $mol_{surface\ Cu}$ s^{-1}) using the formula: CTY*M_{Cu}/D_{Cu}, in which M_{Cu} stands for the molecular weight of Cu and D_{Cu} the fraction of surface Cu atoms. The value of D_{cu} is calculated from the Cu d_s, assuming fully accessible and spherical particles using the formula $6*(V_{Cu}\ A_{Cu}^{-1})/d_s$. Herein, A_{Cu} is the molar area occupied by surface Cu atoms ($4.10*10^{22}$ nm^2) and V_{Cu} is the molar volume occupied by bulk Cu atoms ($7.09*10^{21}$ nm^3). D_{Cu} is thus calculated as $1.04/d_s$, with d_s in nm [39]. The initial TOF at 180 °C was determined after around 30 h on stream, and calculated from the Cu d_s of the fresh Cu/C catalyst. The final TOF at 180 °C was calculated after around 150 h on steam, and calculated from the Cu d_s after catalysis. To be concise, the initial reaction times will be referred to as 30 and 50 h on stream, yet precise reaction times may vary ± 2.5 h depending on moment of GC sampling.

The E_a and A values in the Arrhenius model were obtained from the slope of a linear fit line through the ln(r) values and the intercept with the y-axis, respectively. Herein, the rate r was either defined as CTY ($mmol_{EtOH}$ $g_{Cu}^{-1}h^{-1}$) or surface-normalized CTY ($mmol_{EtOH}$ $m_{Cu}^{-2}h^{-1}$) at conversions of ethyl acetate < 25%. In the Arrhenius model, the CTY at 180 °C was determined from the final isothermal stage, to minimize the influence of initial activation during the first 30 h on stream. Further details on method for catalyst testing are described in Section S2 of the Supporting Information.

3. Results & discussion

3.1. Tuning the Cu particle size

A series of carbon-supported Cu (Cu/C) catalysts was prepared, using incipient wetness impregnation of a graphite support, followed by drying and thermal treatment to decompose the Cu $(NO_3)_2$ precursor. Two methods to tune the Cu particle size were applied. First, variation of the Cu loading between 6 and 12 wt% led to control over the Cu particle size between 8 and 14 nm, using a pristine carbon support. In the second approach, liquid phase HNO_3 oxidation of the carbon support was employed to efficiently introduce oxygen-containing surface groups [37]. Using the oxidized carbon support and varying the final heat treatment temperature between 250 and 400 °C, allowed us to control the Cu particle size between 3 and 7 nm. Powder X-ray diffractometry confirmed the particle size analysis by TEM for all Cu/C catalysts. Combining these synthesis approaches allowed use to tune the Cu particle size between 3 and 14 nm. The Cu/C catalysts in this study were denoted as *X*_Cu/*Y*, in which *X* shows the surface-averaged Cu particle size in nm and *Y* indicates the type of carbon material. The physicochemical properties for the full series of Cu/C catalysts were summarized in Table 1.

To assess the influence of the support functionalization on catalyst stability, we prepared three Cu/C catalysts with the same Cu particle size, but using different Cu loadings (6.3 or 16.4 wt%) and/or support materials (pristine or oxidized carbon). The first sample was prepared using 6.3 wt% Cu and pristine carbon as the support. After heating to 230 °C in 20 vol% H_2/N_2, Cu particles of 8.6 nm were obtained (8.6_Cu/PC; Fig. 1a). The second sample was prepared using the same Cu loading (6.3%), but using oxidized carbon as the support. In general, oxidizing the carbon support leads to smaller particles. To obtain the same Cu particle size of around 8 nm, the second sample had to be heated to 400 °C in a flow of 5 vol% H_2/N_2, which resulted in Cu particles of 7.3 nm (7.3_Cu/OC; Fig. 1b). The third sample was prepared using a higher Cu loading (16.4%) on the oxidized carbon support. This sample was heated to only 230 °C, yielding 8.0 nm Cu particles (8.0_Cu/OC; Fig. 1c). The Cu particle size was ~8 nm for the three different Cu/C catalysts, with similar particle size distributions (Fig. 1d) and poly-dispersity indexes (PDI) or around 33–34% (Table 1). However, the estimated interparticle distance (d_{Cu-Cu}) was significantly higher for the Cu/C catalysts with the lowest Cu loading, for example 38 nm for the 8.6_Cu/PC catalyst with 6.3 wt% Cu, compared to 16 nm for the 8.0_Cu/OC catalyst with 16.1 wt% Cu. XRD studies on the reduced Cu/C catalysts (Fig. 1e), showed similar Cu^0 crystallite sizes between 6.0 and 7.3 nm. The Cu/C catalyst with 16.4 wt% Cu exhibited the most intense Cu^0 (2 0 0) diffraction peak, which was expected since it contains the highest Cu loading. These examples illustrate how we can control the Cu particle size by tuning the synthesis parameters, and allowed us to assess the influence of the carbon pre-treatment and interparticle distance on stability during catalysis.

3.2. Impact of Cu particle size on catalyst performance

Fig. 2 shows the EtOAc conversion and Cu-normalized time yield (CTY) for several representative Cu/C catalysts at 180–210 °C. The CTY after 30 and 150 h on stream are presented in Table S1 for all 12 Cu/C catalysts. In all cases, the conversion increased during the first 30 h on stream (Fig. 2a). Initial changes in activity are common for Cu-catalyzed hydrogenation reactions

Table 1
Physicochemical properties of the series of Cu/C catalysts with varying Cu particle size.

Catalyst[a]	Cu loading (wt%)	T^b (°C)	$d^0_{Cu\ XRD}$ (nm)	$d_n \pm \sigma_{dn}$ (nm)[c]	$d_s \pm \sigma_{ds}$ (nm)[d]	PDI (%)[e]	Estimated $d_{Cu\text{-}Cu}$ (nm)[f]
3.1_Cu/OC	6.3	250	2.0	2.6 ± 0.8	3.1 ± 0.9	29	7
4.2_Cu/OC	6.3	330	2.6	3.7 ± 1.0	4.2 ± 1.1	26	12
5.2_Cu/OC	6.3	350	4.2	4.3 ± 1.4	5.2 ± 1.6	31	17
7.3_Cu/OC	6.3	400	6.0	5.9 ± 1.6	7.3 ± 2.4	33	29
8.0_Cu/OC	16.4	230	7.1	6.6 ± 2.2	8.0 ± 2.7	34	16
8.6_Cu/PC	6.3	230	7.3	6.8 ± 2.4	8.6 ± 2.9	34	38
9.1_Cu/PC	7.0	230	7.3	6.5 ± 2.9	9.1 ± 3.8	42	39
9.5_Cu/PC	8.0	230	5.5	6.5 ± 3.9	9.5 ± 4.7	49	38
9.8_Cu/PC	9.0	230	6.0	6.8 ± 4.0	9.8 ± 5.0	51	37
10.0_Cu/PC	10.0	230	8.9	7.8 ± 3.2	10.0 ± 3.8	38	35
11.7_Cu/PC	11.0	230	10.2	8.5 ± 3.9	11.7 ± 5.1	44	43
13.4_Cu/PC	11.7	230	10.9	8.9 ± 4.3	13.4 ± 6.2	46	51

a) Carbon-supported Cu catalysts denoted as X_Cu/Y, in which X indicates the surface-averaged Cu particle size in nm by TEM, and Y denotes the type of carbon support material, i.e. either pristine carbon (PC) or oxidized carbon (OC); b) Heat treatment temperature for reduction during catalyst synthesis; c) Cu number-averaged particle size (d_n) calculated as $\sum_{i=1}^{N} d_i / \sum_{i=1}^{N}$ and d) surface-averaged particle size (d_s) calculated as $\sum_{i=1}^{N} d_i^3 / \sum_{i=1}^{N} d_i^2$ where d_i indicates the particle diameter by TEM, including standard deviations in the width of the particle size distributions (σ_{dn} and σ_{ds}); e) Poly-dispersity index (PDI) calculated as σ_{ds}/d_s; f) Estimated average interparticle distance between the surface of individual Cu nanoparticles, assuming a hemispherical Cu particle shape.

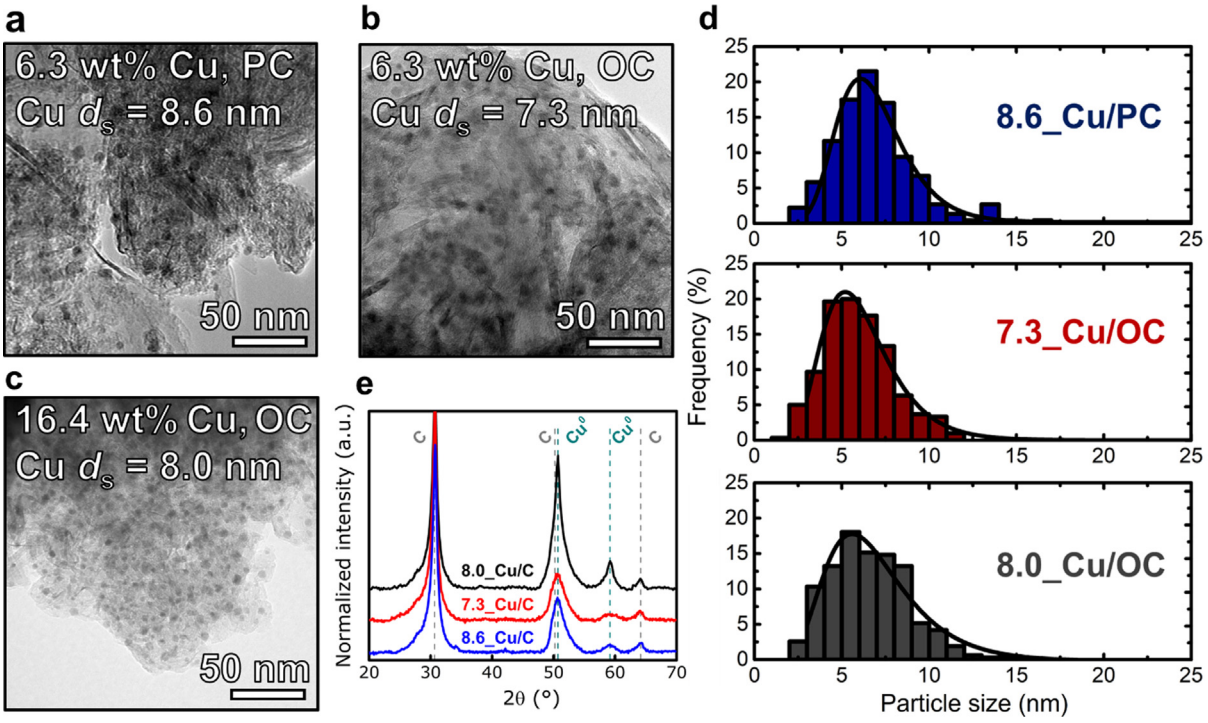

Fig. 1. Characterization of the carbon-supported Cu catalysts with Cu particle size around 8 nm, displaying transmission electron micrographs for a) 6.3 wt% Cu on pristine carbon (PC); b) 6.3 wt% Cu on oxidized carbon (OC) and c) 16.4 wt% Cu on oxidized carbon (OC). d) Cu particle size distributions by TEM, with lognormal fits; e) X-ray diffractograms were normalized to the intensity of the carbon (0 0 2) diffraction peak, carbon baseline subtracted and stacked with individual offset for visual clarity.

are generally believed to be caused by catalyst restructuring [40–42]. The surface restructuring may result in either activation or deactivation, depending on the specific reaction conditions, such as temperature gas atmosphere and catalyst pre-treatment. The 11.7 nm Cu/C catalyst did not show significant particle growth over the course of the experiment, and therefore the initial increase in conversion was not ascribed to Cu particle growth, yet rather to Cu surface restructuring and equilibration of the surface adsorbate composition. Catalyst stability was evaluated by comparing the conversions after 30 and 150 h on stream, both at 180 °C. Only minor changes in conversion were observed during catalysis. Overall, the highest conversion was observed for Cu particles of around 6 nm (Table S1). Remarkably, the selectivity towards ethanol (S_{EtOH}) was > 99.5% for all Cu/C catalysts, with ethane and acetaldehyde as the main by-products. It was significantly higher than reported values in literature for supported Cu-based catalysts, which are typically ~95% in the same temperature and conversion range [10,14,17,18]. The superior selectivities for the Cu/C catalysts are ascribed to the chemically inert nature of the carbon support [37,43].

Adsorption/desorption studies of ethyl acetate on carbon materials have been reported in literature and a fairly strong interaction has been found [44–46]. However, the experiments in literature used predominantly microporous carbon materials and lower temperatures than those relevant for catalysis. The surface coverage of ethyl acetate on carbon under catalysis reaction conditions is hence likely low. If a bifunctional mechanism would play an important role, the specific interface between the Cu nanoparticles and the support becomes an important parameter, and it is expected that smaller metal particles will give more active

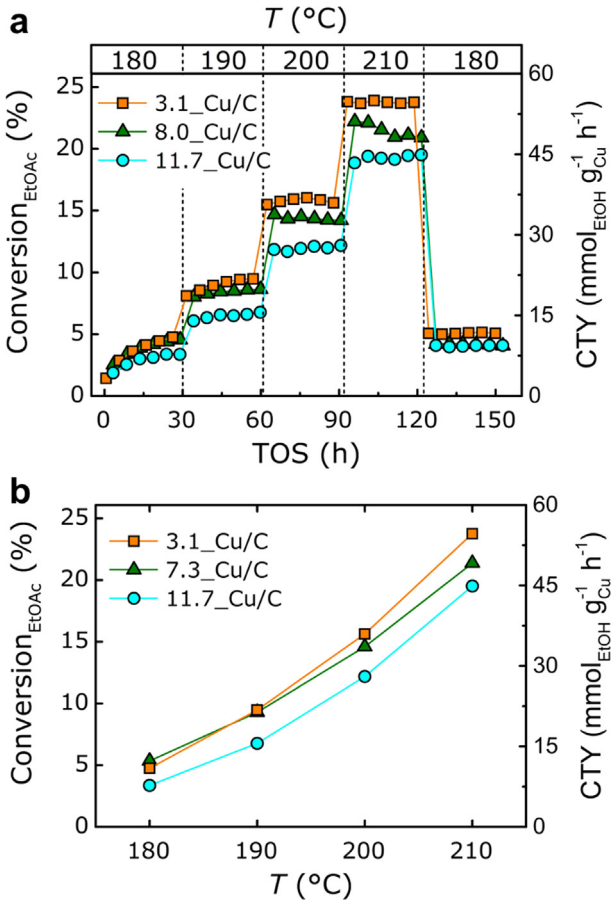

Fig. 2. EtOAc conversion and Cu-normalized time yield (CTY), for three representative Cu/C catalysts of various Cu particle sizes, with a) conversion as a function of time on stream (TOS) at different temperatures and b) conversion over different temperature, at the end of each isothermal stage (30, 60, 90 and 120 h on stream). Reaction conditions: H_2:EtOAc:He = 10:1:1 M ratio, 180–210 °C and 30 bar(g).

catalysts, while we find the opposite for our catalysts. Hence, it is unlikely that the carbon support plays an important role in catalysis. Two reference measurements using either the bare pristine or bare oxidized carbon supports showed no ethyl acetate conversion at 210 °C, thus excluding hydrogenation activity on the bare carbon supports, supporting that the hydrogenation of ethyl acetate only occurs on the Cu particle surface.

Next, we assessed the Cu particle growth during catalysis. Particle growth is known to be a main deactivation mechanism for Cu-based catalysts, and can be affected by the Cu particle size, the poly-dispersity in particle size distribution, the interparticle distance, and hence the Cu loading [47–51]. Here, we discern the influence of two main mechanisms for particles growth, i.e. particle diffusion followed by coalescence, and Ostwald ripening, as schematically depicted in Fig. 3a. We compared the Cu particle size for the fresh and used Cu/C catalysts after 150 h on stream (Fig. 3b). No significant influence of the carbon support surface-oxidation treatment was observed. However, the smallest Cu particles grew consistently more than the larger Cu particles. For example, the 3.1 nm particles grew to 7.0 nm after 150 h catalysis, while the 13.4 nm particles did not significantly grow. The faster growth of the smallest Cu particles is possibly due to the typically shorter interparticle distances for the smallest Cu particles, *e.g.* 7 nm for 3.1_Cu/C and 51 nm for 13.4_Cu/C (Table 1).

The stability for the three Cu/C catalysts with particle size ~8 nm (7.3_Cu/OC, 8.0_Cu/OC and 8.6_Cu/PC) was compared (Section S2). Of these catalysts, the interparticle distance was the largest for the 8.6_Cu/PC catalyst, which also showed the most stable conversion over time and least particle growth. The poly-dispersity index increased with increasing particle size, *e.g.* 29% for 3.1_Cu/OC and 46% for 13.4_Cu/PC (Table 1). Considering the fact that the largest particles with the largest poly-dispersity were the most stable in size, Ostwald ripening was excluded as a main growth mechanism as it is strongly enhanced by high poly-dispersities [51]. Coalescence was therefore assumed to be the main pathway for particle growth, as it strongly depends on the interparticle distance [50,52].

The relationship between turn-over frequency (TOF) and Cu particle size is displayed in Fig. 4. Both the initial and final Cu particle sizes were correlated to the activities after the 30 and 150 h on stream, respectively. Limited particle growth is expected during the initial activation period of 30 h at 180 °C, since particle growth is known to be accelerated at elevated temperatures. The good correlation between initial and final TOF values around the same Cu particle same validate our approach, and allow us to determine the TOF from 3 to 14 nm. The TOF increased around 4-fold for increasing Cu particle size from 3 to 10 nm, i.e. $0.6*10^{-3}$ s^{-1} for the 3 nm Cu particles, up to $2.0*10^{-3}$ s^{-1} for 10 nm Cu particles. For Cu particles above 10 nm, the TOF was size-independent. This is the first report on the Cu particle size effects for EtOAc hydrogenation, and it demonstrates that the reaction is sensitive to the Cu particle size below 10 nm. A similar 4-fold increase in activity with increasing Cu particle size below 10 nm was recently observed for the Cu-catalyzed methanol synthesis reaction [8]. Even though the EtOAc, CO and CO_2 reactants are distinctly different in chemical nature, the proposed rate-determining steps are quite similar, *i.e.* hydrogenation of the acyl intermediate for EtOAc hydrogenation [30,31] and formate hydrogenation in methanol synthesis [14]. These similar trends suggest a common active site for both reactions. Interestingly, the Cu particle size effects are moderate compared to the ~10-fold increase in Fischer-Tropsch activity for increasing Co particle size from 2 to 6 nm [3], and ~10-fold increase in ammonia synthesis activity for Ru particles increasing from 1 to 6 nm [21,53]. For the Fischer Tropsch and ammonia synthesis reactions, the rate-determining steps are not surface hydrogenation reactions, but rather the dissociation of CO and N_2, respectively. These findings show that the chemical reactivity does not only depend on the nature of the active site, but is also correlated to the nature of the intermediates for the rate-determining step [21].

The Cu/C catalysts were significantly more active than previously reported un-promoted Cu catalysts. For example, Lu and co-workers described TOF values of just $0.8*10^{-3}$ s^{-1} at 280 °C, for 13–23 nm Cu catalysts supported on SiO_2, Al_2O_3 and ZrO_2 [17], while we measured TOF between 0.2 and $2.2*10^{-3}$ s^{-1} at 180 °C. The different synthesis methods may play a crucial role. The Cu catalysts on SiO_2, Al_2O_3 and ZrO_2 were prepared using Na_2SiO_3 and Na_2CO_3 reagents [17], whilst it is known that Na^+ may poison the Cu surface in hydrogenation reactions [54]. Another explanation for the higher TOF in this study may be the water content in the EtOAc reactant. Karl Fischer titration showed that the water concentration in our study was<50 ppm. The purity of the EtOAc feed can have a strong influence on the catalytic performance [47,55], and may explain the superior activity of the Cu/C catalysts under our experimental conditions.

3.3. Origin of Cu particle size effect

In general, particle size effects may be caused by size-dependent changes in the electronic nature, metal-support interactions and the particle surface structure. All Cu/C catalyst contained Cu particles of 2 nm or larger, for which electronic support effects are expected to be negligible [24]. Moreover, carbon only weakly

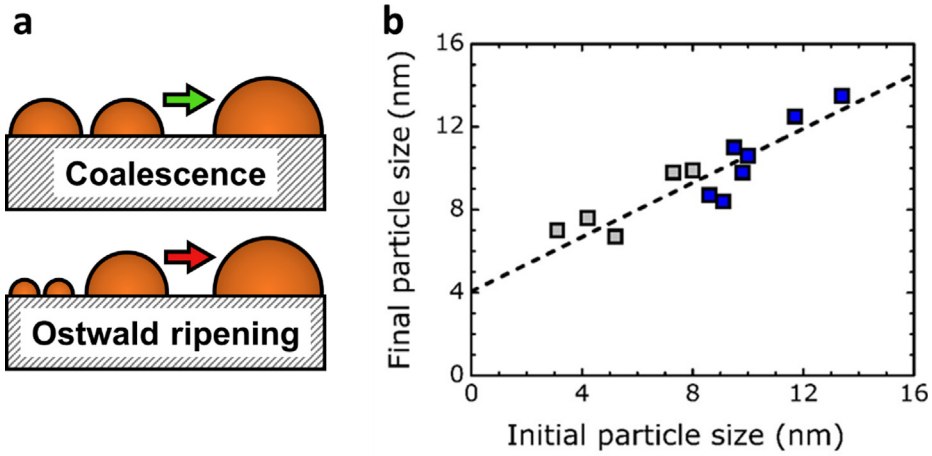

Fig. 3. a) Schematic illustration of the two main mechanisms for particle growth, through coalescence and Ostwald ripening. b) Correlation between the initial and final Cu surface-averaged particle sizes after 150 h on stream, for the full series of Cu/C catalysts prepared using pristine carbon (blue) or oxidized carbon (gray) as the support.

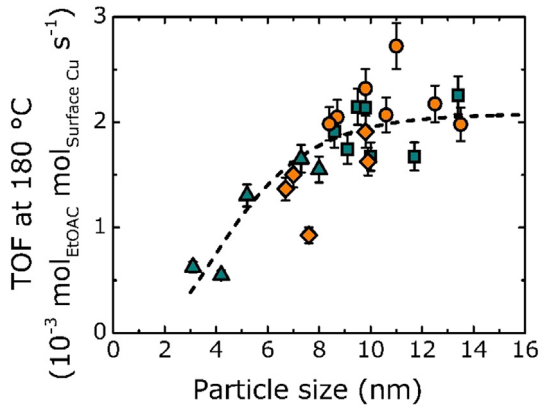

Fig. 4. Turn-over frequencies (TOF) 180 °C and 30 bar(g), as a function of the surface-averaged Cu particle size. Both TOF after 30 h on stream (cyan symbols) and after 150 h on stream (orange symbols) are displayed as independent data points, which were correlated to the Cu particle size of the fresh and used catalysts, respectively. The Cu catalysts were prepared using either pristine graphite (circle and square symbols) or oxidized graphite (triangle and diamond symbols) as the support material. An exponential curve was fitted as a trendline for the TOF values. The error bars represent the relative standard deviation in TOF, which was only 8% and therefore error bars may lie behind the data markers. Reaction gas mixture as H_2:EtOAc:He in 10:1:1 M ratio.

interacts with the Cu particles. Therefore, metal-support interaction is an unlikely origin of the observed particle size effects. We evaluated the catalyst reducibility, by H_2 temperature-dependent reduction analysis on the passivated Cu/C catalysts (Fig. S3). All catalysts were completely reduced to Cu^0/C at 200 °C under a flow of 5 vol% H_2/Ar. The largest change in the reduction temperatures was observed for increasing Cu particle size from 3 to 5 nm. Above 5 nm, the reduction temperatures did not strongly change. Hence, it is unlikely that the reducibility explains the observed Cu particle size effect. Next, we examined the role of water. In our experiments, the formation of ethane (<0.5% product selectivity) coincided with water production (<100 ppm in the gas-phase). Based on calculations of simulated reaction conditions on bulk Cu, we expect an equilibrium in $Cu/Cu^+/Cu^{2+}$ oxidation states, with less than 1 in 10^5 Cu atoms being present as Cu^+ or Cu^{2+} (see section S3 for details). Although the fraction is likely higher for nanoparticulate Cu, the results suggest that electronic effects are unlikely to explain the particle size dependence in catalytic activity.

The apparent activation energy (E_a) was calculated using the Arrhenius model (Fig. S4). In order to determine the E_a, it is important to consider the reaction kinetics. From literature it is known that for a 10-fold excess of H_2 over EtOAc, between 190 and 300 °C, the reaction orders with respect to both H_2 and EtOAc were close to zero, indicating a saturated surface coverage [9–11,14]. Accordingly, a zeroth order dependency of the EtOAc concentration on the reaction rate was assumed. The E_a was determined from rates (rather than rate constants) over the temperature range of 180–210 °C. We used the EtOAc conversion at the final stage at 180 °C (after 150 h) to minimize the influence of the catalyst activation behavior. The E_a was calculated independently as a function of both the initial and final particle sizes (Fig. 5a). The apparent E_a ranged between 89 and 103 kJ mol^{-1}, with an average value of 94 kJ mol^{-1}. Fascinatingly, the E_a for the Cu/C catalyst was hence found to be independent of the Cu particle size. Although the exact value of E_a depends on specific reaction conditions such as temperature and pressure, the results for Cu/C are in good agreement with reported values of 74 kJ mol^{-1} for Cu/ZrO_2 [29], 107 kJ mol^{-1} for Cu/SiO_2 [11], 88 kJ mol^{-1} for Raney Cu [9] and 119 kJ mol^{-1} for macroscopic Cu [10]. This confirms that electronic effects scaling with size are not the cause of the Cu particle size effects, but rather due to an increase in relative abundance of the active sites with increasing size.

We also calculated the pre-exponential factor (A), which can be correlated to the number of active sites for catalysis, assuming that their nature does not change with size (Fig. 5b). The value of A was derived from the Arrhenius model using the surface-normalized CTY, defined as $mmol_{EtOH}\ m_{Cu}^{-2}h^{-1}$ and using an averaged E_a of 94 kJ mol^{-1}. An approximate 4-fold increase in A was observed for Cu particles between 3 and 10 nm (from $0.8*10^{10}$ to $3.2*10^{10}$), correlating to the 4-fold increase in TOF for the same particle size range. This indicates the presence of a well-defined and size-independent active Cu site responsible for EtOAc conversion, for which the abundance increased with increasing particle size up to around 10 nm.

3.4. Nature of the active site

To evaluate the nature of the catalytic site, we need to consider the Cu surface structure. The particle shape and surface structure of face centered cubic metal nanoparticles are known to be size-dependent [1,22,56]. To describe the complete surface nature of Cu particles up to 16 nm, we extrapolated the models by Van Hardeveld [22] and Van Helden [1] (details provided in Section S4). The Cu surface mainly consists of (1 1 1) and (1 0 0) facets with exposed terrace sites, but also exhibits different defects sites with lower coordination numbers such as corner, edge, step and kink

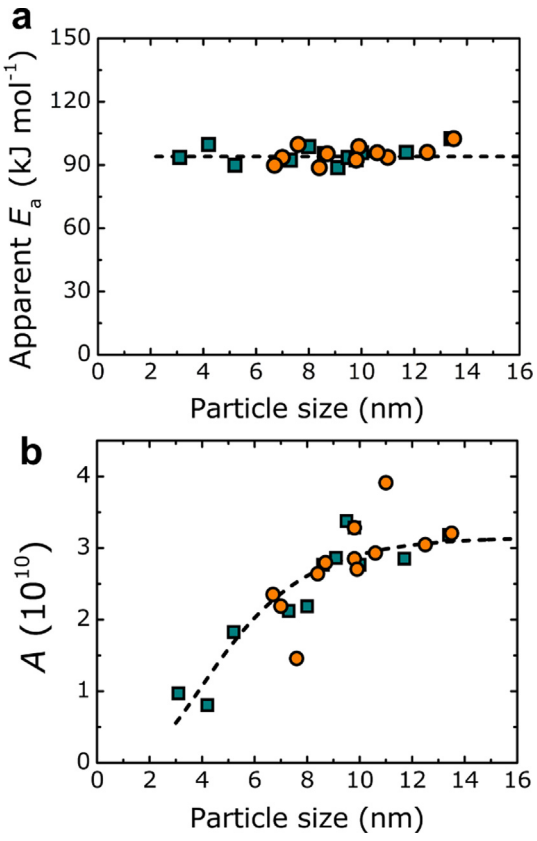

Fig. 5. a) Apparent activation energy (E_a) and b) pre-exponential factor (A) displayed as a function of the surface-averaged Cu particle size. The A values were derived from the Arrhenius model using r as the surface-normalized reaction rate, i.e. $mmol_{EtOH}\ m_{Cu}^{-2}h^{-1}$. The E_a and A values were displayed both after 30 h on stream (cyan squares) and after 150 h on stream (orange circles), as independent data points. Reaction conditions: H_2:EtOAc:He = 10:1:1 M ratio, 180–210 °C and 30 bar (g).

sites. In general, the surface sites with the lowest coordination numbers exhibit the highest adsorption strengths [27]. The different surface sites therefore may have distinctly different chemical reactivities.

We compared the size-dependence of the TOF with the abundance of each type of surface site. The fractions of corner and edge sites decreased with increasing Cu particle size above 2 nm, and were therefore excluded as the active site for the hydrogenation reaction. The corner and edge sites are likely too small to accommodate both dissociated hydrogen and the oxygenate intermediates [21,24,25,57]. The fractions of Cu (1 1 1) and Cu (1 1 0) terrace sites steeply increased with increasing Cu particle size up to around 6 nm, and are hence unlikely to strongly contribute to the catalytic activity. Interestingly, the fraction of step and kink sites gradually increases up to around 8–10 nm, thus closely matching the experimental TOF values (Fig. 6). The B5A step, B5B step and B6 kink sites can be found at the interface of different Cu (1 1 1) and Cu (1 0 0) planes, which represent the geometrical equivalent of higher Miller index Cu (3 1 1), Cu (2 2 1) and Cu (3 2 1) surfaces, respectively [1,22]. The differences between the theoretical fraction of step and kink sites and experimental TOF values may originate from structural deviations between the free-standing particle models and actual supported Cu particles under reaction conditions. The coordination saturation and adsorption strengths for the B5A and B5B step sites and B6 kink sites are reported to be similar to each other [1], hence it was not possible to unequivocally distinguish between the three sites. The adsorption strength likely has a strong influence on the hydrogenation activity. In line with Sabatier's Principle, we propose that both the step and kink sites (with intermediate coordination saturation and adsorption strength) are responsible for the Cu-catalyzed hydrogenation of ethyl acetate.

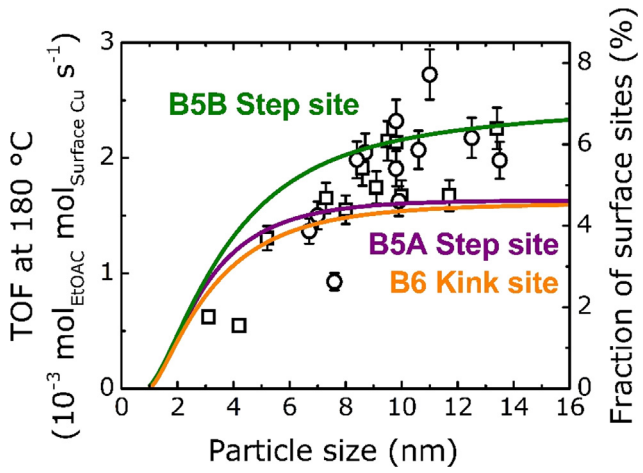

Fig. 6. Turn-over frequencies (TOF) and the theoretical fraction of Cu step and kink surface sites, as a function of the surface-averaged Cu particle size. Both TOF after 30 h on stream (empty squares) and after 150 h on stream (empty circles) are displayed as independent data points, which were correlated to the Cu particle size of the fresh and used catalysts, respectively. The error bars represent the relative standard deviation in TOF, which was only 8% and therefore error bars may lie behind the data markers. Reaction gas mixture as H_2:EtOAc:He in 10:1:1 M ratio. The fractions of the different Cu surface sites were calculated by extrapolation of the particle models by Van Hardeveld [22] and Van Helden [1] for fcc metals.

This is the first systematic study on the impact and origin of Cu particle size effects for the hydrogenation of EtOAc. Investigating the nature of the active site for the Cu-catalyzed hydrogenation reaction, was greatly facilitated here by using carbon as a support material. We showed that the relative abundance of step sites scales with both our measured pre-exponential factor in the Arrhenius model and TOF values, and therefore propose structure sensitivity as the origin of the observed Cu particle size-activity relationships. A maximum conversion was obtained with Cu particles of around 6 nm, which may guide the performance optimization of Cu-based catalysts for a plethora of hydrogenation reactions.

4. Conclusions

The effects of Cu particle size between 3 and 14 nm were investigated for the Cu-based hydrogenation of ethyl acetate. High surface area graphite was used as an inert catalyst support, to investigate the intrinsic Cu particle size effects. The catalysts with Cu particles of 8 nm or larger were the most stable in this study. The TOF increased approximately 4-fold when increasing the Cu particle size from 3 to 10 nm, and became size-independent for particles above 10 nm. The apparent activation energy was independent of the Cu particle size, suggesting that the nature of the active site did not change with Cu particle size. However, the pre-exponential factor in the Arrhenius model suggested that relative abundance of the active site increased with Cu particle size up to 10 nm, which was ascribed to a size-dependent increase in the fraction of step and kink surface sites. A maximal yield was obtained with Cu particles of around 6 nm, giving an optimal balance between intrinsic activity and available surface area as a function of Cu particle size.

Declaration of Competing Interest

The authors declare that they have no known competing financial interests or personal relationships that could have appeared to influence the work reported in this paper.

Acknowledgements

This work was supported by BP for funding RB, ERC (grant number ERC-2014-CoG-648991) for additional funding for PEdJ, and ERC (grant number ERC-AG338846) for additional funding for KPdJ and supporting the transmission electron microscopy facilities. The authors thank Lennart Weber, Remco Dalebout, Neil Sainty and Roy Partington for technical support in the catalytic experiments.

Appendix A. Supplementary material

Supplementary data to this article can be found online at https://doi.org/10.1016/j.jcat.2020.05.006.

References

[1] P. Van Helden, I.M. Ciobîcă, R.L.J. Coetzer, The size-dependent site composition of FCC cobalt nanocrystals, Catal. Today 261 (2016) 48–59.
[2] H.M. Torres Galvis, J.H. Bitter, T. Davidian, M. Ruitenbeek, A.I. Dugulan, K.P. de Jong, Iron particle size effects for direct production of lower olefins from synthesis gas, J. Am. Chem. Soc. 134 (2012) 16207–16215.
[3] J.P. Den Breejen, P.B. Radstake, G.L. Bezemer, J.H. Bitter, V. Frøseth, A. Holmen, K.P.D. Jong, On the origin of the cobalt particle size effects in fischer−tropsch catalysis, JACS 131 (2009) 7197-7203.
[4] L.J. Durndell, C.M.A. Parlett, N.S. Hondow, M.A. Isaacs, K. Wilson, A.F. Lee, Selectivity control in Pt-catalyzed cinnamaldehyde hydrogenation, Sci. Rep. 5 (2015) 9425.
[5] R. Van Hardeveld, A. van Montfoort, The influence of crystallite size on the adsorption of molecular nitrogen on nickel, palladium and platinum: An infrared and electron-microscopic study, Surf. Sci. 4 (1966) 396–430.
[6] J.E. van den Reijen, S. Kanungo, T.A.J. Welling, M. Versluijs-Helder, T.A. Nijhuis, K.P. de Jong, P.E. de Jongh, Preparation and particle size effects of Ag/α-Al2O3 catalysts for ethylene epoxidation, J. Catal. 356 (2017) 65–74.
[7] M.B. Gawande, A. Goswami, F.-X. Felpin, T. Asefa, X. Huang, R. Silva, X. Zou, R. Zboril, R.S. Varma, Cu and Cu-based nanoparticles: synthesis and applications in catalysis, Chem. Rev. 116 (2016) 3722–3811.
[8] R. Van den Berg, G. Prieto, G. Korpershoek, L.I. van der Wal, A.J. van Bunningen, S. Lægsgaard-Jørgensen, P.E. de Jongh, K.P. de Jong, Structure sensitivity of Cu and CuZn catalysts relevant to industrial methanol synthesis, Nat. Commun. 7 (2016) 13057.
[9] J.W. Evans, M.S. Wainwright, N.W. Cant, D.L. Trimm, Structural and reactivity effects in the copper-catalyzed hydrogenolysis of aliphatic esters, J. Catal. 88 (1984) 203–213.
[10] P. Claus, M. Lucas, B. Lücke, T. Berndt, P. Birke, Selective hydrogenolysis of methyl and ethyl acetate in the gas phase on copper and supported Group VIII metal catalysts, Appl. Catal. A 79 (1991) 1–18.
[11] A.K. Agarwal, N.W. Cant, M.S. Wainwright, D.L. Trimm, Catalytic hydrogenolysis of esters: a comparative study of the reactions of simple formates and acetates over copper on silica, J. Mol. Catal. 43 (1987) 79–92.
[12] D.S. Brands, E.K. Poels, A. Bliek, Ester hydrogenolysis over promoted Cu/SiO2 catalysts, Appl. Catal. A 184 (1999) 279–289.
[13] W. Zhou, J. Kang, K. Cheng, S. He, J. Shi, C. Zhou, Q. Zhang, J. Chen, L. Peng, M. Chen, Y. Wang, Direct conversion of syngas into methyl acetate, ethanol, and ethylene by relay catalysis via the intermediate dimethyl ether, Angew. Chem. Int. Ed. 57 (2018) 12012–12016.
[14] M.A.N. Santiago, M.A. Sanchez-Castillo, R.D. Cortright, J.A. Dumesic, Catalytic reduction of acetic acid, methyl acetate, and ethyl acetate over silica-supported copper, J. Catal. 193 (2000) 16–28.
[15] Y. Liu, K. Murata, M. Inaba, I. Takahara, Synthesis of ethanol from methanol and syngas through an indirect route containing methanol dehydrogenation, DME carbonylation, and methyl acetate hydrogenolysis, Fuel Process. Technol. 110 (2013) 206–213.
[16] B.J. Daniel, J.M.S. Deeley, B.P. Gracey, C.R. Li, WO2009063173.
[17] Z. Lu, H. Yin, A. Wang, J. Hu, W. Xue, H. Yin, S. Liu, Hydrogenation of ethyl acetate to ethanol over Cu/ZnO/MOx (MOx=SiO2, Al2O3, and ZrO2) catalysts, J. Ind. Eng. Chem. 37 (2016) 208–215.
[18] X. Ma, Z. Yang, X. Liu, X. Tan, Q. Ge, Dynamic redox cycle of Cu0 and Cu+ over Cu/SiO2 catalyst in ester hydrogenation, RSC Adv. 5 (2015) 37581–37584.
[19] P. Munnik, P.E. de Jongh, K.P. de Jong, Recent developments in the synthesis of supported catalysts, Chem. Rev. 115 (2015) 6687–6718.
[20] K.P. De Jong, Synthesis of solid catalysts, Wiley, 2009.
[21] R.A. Van Santen, Complementary structure sensitive and insensitive catalytic relationships, Acc. Chem. Res. 42 (2009) 57–66.
[22] R. Van Hardeveld, F. Hartog, The statistics of surface atoms and surface sites on metal crystals, Surf. Sci. 15 (1969) 189–230.
[23] C. Vogt, E. Groeneveld, G. Kamsma, M. Nachtegaal, L. Lu, C.J. Kiely, P.H. Berben, F. Meirer, B.M. Weckhuysen, Unravelling structure sensitivity in CO2 hydrogenation over nickel, Nat. Catal. 1 (2018) 127–134.
[24] B.R. Cuenya, Synthesis and catalytic properties of metal nanoparticles: Size, shape, support, composition, and oxidation state effects, Thin Solid Films 518 (2010) 3127–3150.
[25] C.R. Henry, C. Chapon, S. Giorgio, C. Goyhenex, Size Effects in Heterogeneous Catalysis, in: R.M. Lambert, G. Pacchioni (Eds.), Chemisorption and Reactivity on Supported Clusters and Thin Films: Towards an Understanding of Microscopic Processes in Catalysis, Springer, Netherlands, Dordrecht, 1997, pp. 117–152.
[26] T.E. James, S.L. Hemmingson, C.T. Campbell, Energy of Supported Metal Catalysts: From Single Atoms to Large Metal Nanoparticles, ACS Catal. 5 (2015) 5673–5678.
[27] Z.-P. Liu, P. Hu, General Rules for Predicting Where a Catalytic Reaction Should Occur on Metal Surfaces: A Density Functional Theory Study of C−H and C−O Bond Breaking/Making on Flat Stepped, and Kinked Metal Surfaces, JACS 125 (2003) 1958–1967.
[28] B. Roldan Cuenya, F. Behafarid, Nanocatalysis: size- and shape-dependent chemisorption and catalytic reactivity, Surf. Sci. Rep. 70 (2015) 135–187.
[29] J. Schittkowski, K. Tölle, S. Anke, S. Stürmer, M. Muhler, On the bifunctional nature of Cu/ZrO2 catalysts applied in the hydrogenation of ethyl acetate, J. Catal. 352 (2017) 120–129.
[30] M. Behrens, F. Studt, I. Kasatkin, S. Kühl, M. Hävecker, F. Abild-Pedersen, S. Zander, F. Girgsdies, P. Kurr, B.-L. Kniep, M. Tovar, R.W. Fischer, J.K. Nørskov, R. Schlögl, The Active Site of Methanol Synthesis over Cu/ZnO/Al_2O_3 Industrial Catalysts, Science 336 (2012) 893–897.
[31] K.C. Waugh, Methanol Synthesis, Catal. Today 15 (1992) 51–75.
[32] E.K. Poels, D.S. Brands, Modification of Cu/ZnO/SiO2 catalysts by high temperature reduction, Appl. Cataly. A-General 191 (2000) 83–96.
[33] S. Zheng, K. Zhu, W. Li, Y. Ji, Hydrogenation of dimethyl malonate to 1,3-propanediol catalyzed by a Cu/SiO2 catalyst: the reaction network and the effect of Cu+/Cu0 on selectivity, New J. Chem. 41 (2017) 5752–5763.
[34] A.Y. Yin, X.Y. Guo, W.L. Dai, H.X. Li, K.N. Fan, Highly active and selective copper-containing HMS catalyst in the hydrogenation of dimethyl oxalate to ethylene glycol, Appl. Catal. A-General 349 (2008) 91–99.
[35] J.L. Gong, H.R. Yue, Y.J. Zhao, S. Zhao, L. Zhao, J. Lv, S.P. Wang, X.B. Ma, Synthesis of Ethanol via Syngas on Cu/SiO2 Catalysts with Balanced Cu-0-Cu+ Sites, J. Am. Chem. Soc. 134 (2012) 13922–13925.
[36] M. Mokhtar, C. Ohlinger, J.H. Schlander, T. Turek, Hydrogenolysis of dimethyl maleate on Cu/ZnO/Al2O3 catalysts, Chem. Eng. Technol. 24 (2001) 423–426.
[37] P. Serp, J.L. Figueiredo, Carbon Materials for Catalysis, Wiley, 2008.
[38] A.L. Patterson, The Scherrer Formula for X-Ray Particle Size Determination, Phys. Rev. 56 (1939) 978–982.
[39] G. Ertl, H. Knözinger, J. Weitkamp, Handbook of Heterogeneous Catalysis, Wiley, 2008.
[40] H.H. Kung, Deactivation of methanol synthesis catalysts - a review, Catal. Today 11 (1992) 443–453.
[41] M.B. Fichtl, D. Schlereth, N. Jacobsen, I. Kasatkin, J. Schumann, M. Behrens, R. Schlögl, O. Hinrichsen, Kinetics of deactivation on Cu/ZnO/Al2O3 methanol synthesis catalysts, Appl. Catal. A 502 (2015) 262–270.
[42] G. Prieto, J. Zečević, H. Friedrich, K.P. de Jong, P.E. de Jongh, Towards stable catalysts by controlling collective properties of supported metal nanoparticles, Nat. Mater. 12 (2013) 34–39.
[43] Y. Wang, W. Yang, D. Yao, S. Wang, Y. Xu, Y. Zhao, X. Ma, Effect of surface hydroxyl group of ultra-small silica on the chemical states of copper catalyst for dimethyl oxalate hydrogenation, Catal. Today (2019).
[44] P. Branton, K. Urita, K. Kaneko, Ethyl Acetate Adsorption onto Activated Carbon, Adsorpt. Sci. Technol. 28 (2010) 895–902.
[45] S.D. Manjare, A.K. Ghoshal, Comparison of Adsorption of Ethyl Acetate on Activated Carbon and Molecular Sieves 5A and 13X, J. Chem. Eng. Data 51 (2006) 1185–1189.
[46] L. Gales, A. Mendes, C. Costa, Hysteresis in the cyclic adsorption of acetone, ethanol and ethyl acetate on activated carbon, Carbon 38 (2000) 1083–1088.
[47] M.V. Twigg, M.S. Spencer, Deactivation of supported copper metal catalysts for hydrogenation reactions, Appl. Catal. A 212 (2001) 161–174.
[48] J.A. Moulijn, A.E. van Diepen, F. Kapteijn, Catalyst deactivation: is it predictable?: What to do?, Appl Catal. A 212 (2001) 3–16.
[49] R.-P. Ye, L. Lin, Q. Li, Z. Zhou, T. Wang, C.K. Russell, H. Adidharma, Z. Xu, Y.-G. Yao, M. Fan, Recent progress in improving the stability of copper-based catalysts for hydrogenation of carbon–oxygen bonds, Catal. Sci. Technol. 8 (2018) 3428–3449.
[50] C.H. Bartholomew, Mechanisms of catalyst deactivation, Appl. Catal. A 212 (2001) 17–60.
[51] C.E. Pompe, M. Slagter, P.E. de Jongh, K.P. de Jong, Impact of heterogeneities in silica-supported copper catalysts on their stability for methanol synthesis, J. Catal. 365 (2018) 1–9.
[52] D.M. Argyle, H.C. Bartholomew, Heterogeneous Catalyst Deactivation and Regeneration: A Review, Catalysts 5 (2015).
[53] K. Honkala, A. Hellman, I.N. Remediakis, A. Logadottir, A. Carlsson, S. Dahl, C.H. Christensen, J.K. Nørskov, Ammonia Synthesis from First-Principles Calculations, Science 307 (2005) 555–558.
[54] S.A. Kondrat, P.J. Smith, J.H. Carter, J.S. Hayward, G.J. Pudge, G. Shaw, M.S. Spencer, J.K. Bartley, S.H. Taylor, G.J. Hutchings, The effect of sodium species on methanol synthesis and water–gas shift Cu/ZnO catalysts: utilising high purity zincian georgeite, Faraday Discuss. 197 (2017) 287–307.
[55] M.D. Argyle, C.H. Bartholomew, Heterogeneous Catalyst Deactivation and Regeneration: A Review, Catalysts 5 (2015) 145–269.
[56] T.L. Einstein, Equilibrium Shape of Crystals, Elsevier, 2015.
[57] G.A. Somorjai, K.R. McCrea, J. Zhu, Active Sites in Heterogeneous Catalysis: Development of Molecular Concepts and Future Challenges, Top. Catal. 18 (2002) 157–166.